NJC

Paper

Electronic supplementary information

Layer-structured 3D Nanohybrid MoS_2@rGO on Nickel Foam for High Performance Energy Storage Applications

Ravindra N. Bulakhe[a], Van Hoa Nguyen[b] and Jae-Jin Shim[a*]

[a]School of Chemical Engineering, Yeungnam University, Gyeongsan, Gyeongbuk 38541, Republic of Korea
[b]Department of Chemistry, Nha Trang University, 2 Nguyen Dinh Chieu, Nha Trang, Vietnam

Supplementary information

1) LBL method

A layer by layer (LBL) technique was employed to coat the electrode electrostatically with GO (Fig. **S1**). The GO dispersion was prepared by adding 100 mg in 20 ml deionized water. The GO solution was stirred at 700 rpm for one hour until it become a colloidal suspension. Briefly, the cleaned nickel foam (NF) was dipped in a colloidal GO suspension for 10 min, washed with D.I. water, and dried in an oven. One cycle of this procedure gave a film composed of a monolayer graphene oxide, and repetitive (5–10) cycles, a multilayer GO film. The deposited films were reduced using a reducing agent. Chemical reduction was conducted by dipping multi-layered GO films in an aqueous solution of 0.1 M N_2H_4 (hydrazine) for 24 h at 70° C, followed by washing with D.I. water.

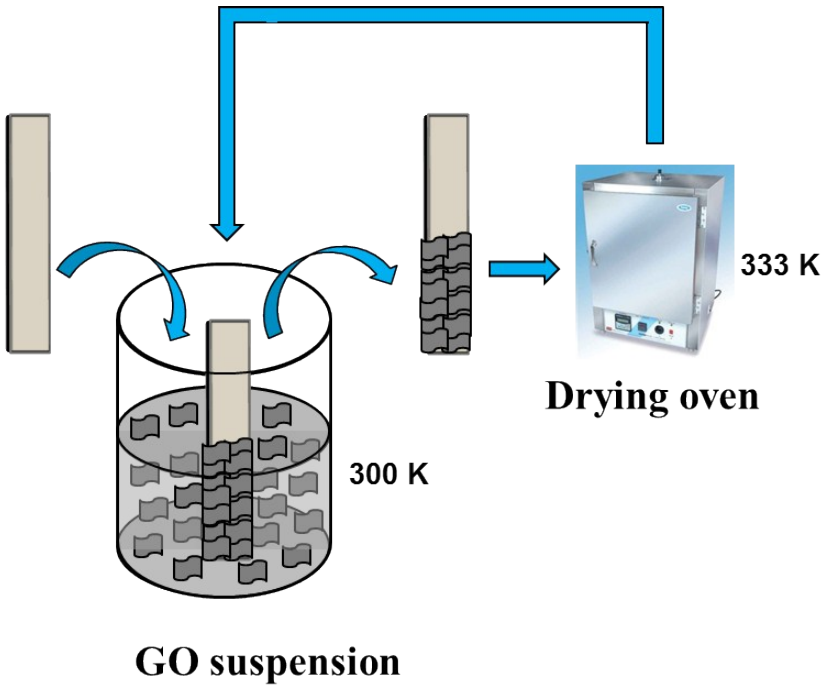

Fig. S1: Schematic of the coating process of GO by LBL method.

2) SILAR method

In 1985, Nicolau introduced the SILAR method (Fig. **S2**) to grow polycrystalline or epitaxial thin films of water-insoluble ionic or covalent compounds of the C_mA_n type by heterogeneous chemical reactions at the solid-solution interface between the adsorbed cations $(CL_p)^{n+}$ and anions $(AL'_q)^{m-}$ according to eq. 1.[1]

$$m(CL_p)^{n+} + n(AL'_q)^{m-} \rightarrow C_mA_n \downarrow + mpL + nqL' \quad \text{.....(1)}$$

where L_p and L'_q are ligands. This method involves the alternative immersion of the current collector in a solution containing a soluble salt of the cation and anion of the compounds to be grown. This aqueous solution phase has been reported for the deposition of MoS_2 on stainless steel substrates to produce large volumes of monolayers and a few layers that can be deposited onto a substrate to form films.

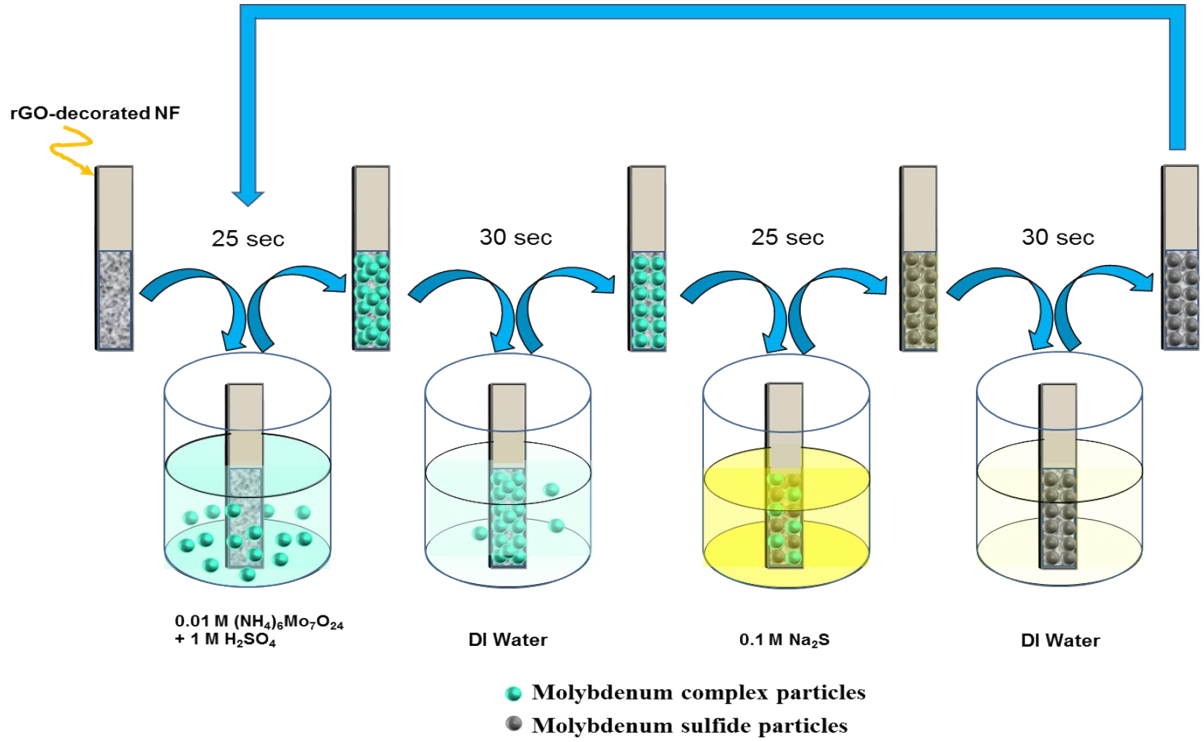

Fig.S2: Schematic diagram of the coating process of MoS2@rGO by SILAR method [2].

Analytical reagent ammonium molybdate [$(NH_4)_6Mo_7O_{24}{\cdot}4H_2O$] and sodium sulfide [$Na_2S{\cdot}H_2O$] were used in the deposition of the MoS_2 3D electrode. The cation precursor was 0.01 M ammonium molybdate solution. The pH was adjusted to 3 by adding dilute sulfuric acid. The source of sulfur ions was 1 M sodium sulfide (pH ~ 13.5). Prepared solutions were taken into beakers and D.I. water was used for rinsing. After every ten deposition cycles, the D.I. water for rinsing was replaced. Deposition was carried out at room temperature (27◦ C) using unstirred reaction solutions. By making several trials of the time durations for adsorption, reaction and rinsing were optimized. The chemically reduced rGO-decorated 3D porous nickel foam (rGO@NF) was immersed in 0.01 M ammonium molybdate for 25 s, and adsorbed ammonium molybdate (molybdenum complex).

The rGO@NF substrate was rinsed with D.I. water for 30 s to remove the desorbed ions. The substrates were immersed in a 0.1 M sodium sulfide solution for 25 s, where the S^{2-} ions were adsorbed and reacted with Mo^{4+} ions on the rGO@NF substrate to decorate with MoS_2 on 3D porous rGO@NF. The unreacted S^{2-} ions were removed by rinsing the substrates in D.I. water for 30 s. By repeating the SILAR deposition cycles 30-50 times, homogeneous, strongly adherent, and compactly stacked MoS_2 layers on NF were obtained.

3) SAED pattern

Fig. S3 shows the selected area energy dispersion (SAED) pattern of MoS_2@rGO electrode, it confirms the polycrystalline nature of the MoS_2@rGO materials.

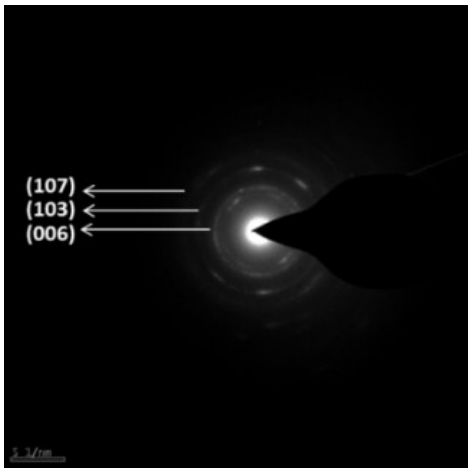

Fig. S3: Selected area energy dispersion (SAED) pattern of MoS_2@rGO electrode.

4) Elemental mapping

In Figs. **S4 (a-d)**, C, Mo, and S were distributed over the same area, verifying the formation of MoS_2 on the rGO surface. The peaks for C, Mo, and S in Fig. **S4 (e)** also confirm the formation of the composite. The peaks around 8 and 9 were formed due to the copper grid that held the sample.

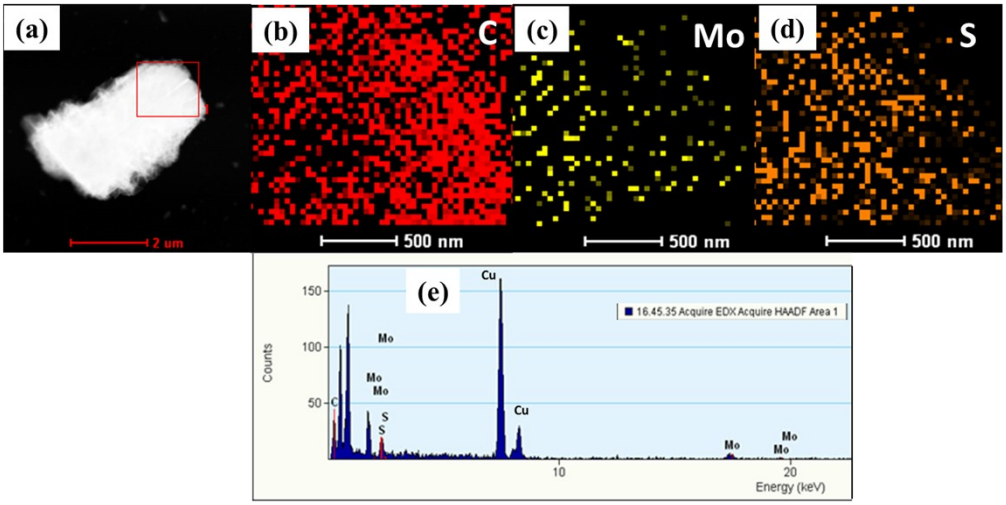

Fig.S4 TEM image of MoS_2@rGO (individual rGO sheet decorated by MoS_2) (a); EDS of C (b), Mo (c), S (d) elemental maps and EDS spectra (e) taken from the same area.

5) Equations for supercapacitor calculations

The specific capacitance C_{sp} was calculated by eq. **S1**:

$$C_{sp} = \frac{\int_{V_1}^{V_2} i\, dV}{(V_2 - V_1)vm} \qquad \textbf{(S1)}$$

where i represents current response to the given voltage (V), V_1 and V_2 are the lower and upper potential limits, respectively, ν is the scan rate, and m is the mass of the electrode.

Specific capacitance from the charge-discharge plot was calculated by eq. **S2**:

$$C_{sp} = \frac{it}{m\Delta v} \qquad \textbf{(S2)}$$

where t is the discharge time and Δv is the potential window. Here, i/m can be replaced by the current density. The energy density (E) and power density (P) were calculated using eqs. **S3** and **S4**:

$$E = \frac{1}{2} C_{sp} (\Delta v)^2 \quad \textbf{(S3)}$$

$$P = \frac{E}{t} \quad \textbf{(S4)}$$

6) EIS study for electrodes after cyclic stability tests

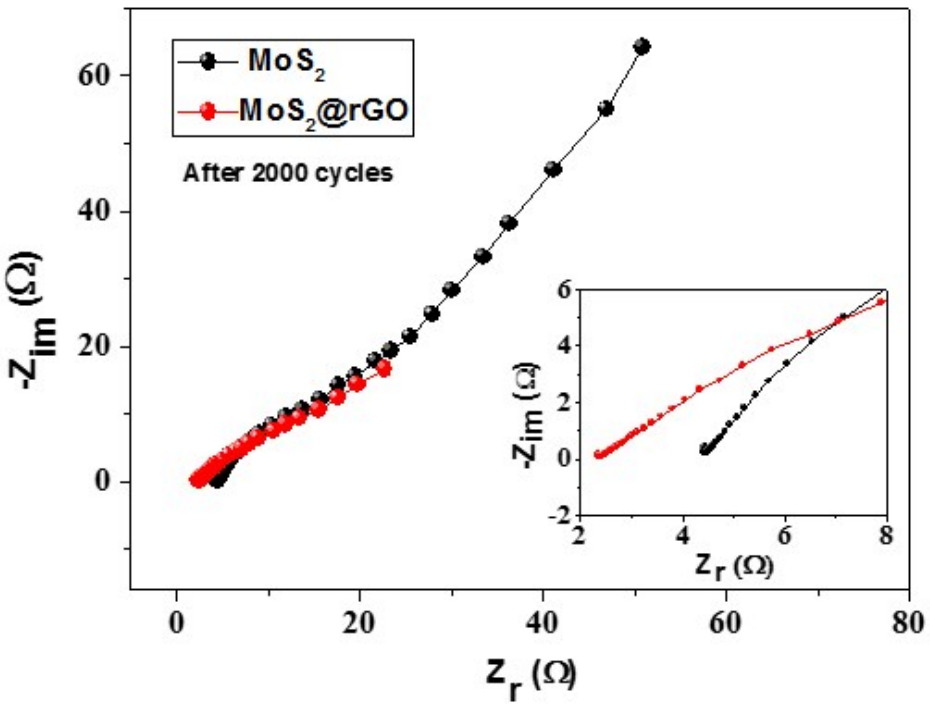

Fig. S5: Nyquist plots of (a) MoS_2 and (b) MoS_2@rGO electrodes after 2000 cycles within the frequency range, 40 kHz to 0.1 Hz.

7) SEM images after cycling

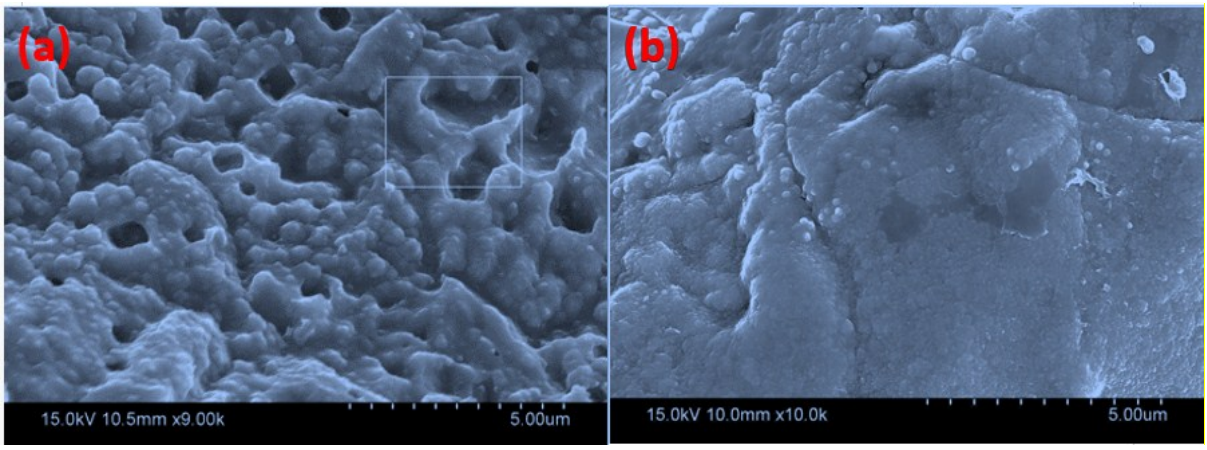

Fig. S6: SEM images of (a) MoS_2 and (b) MoS_2@rGO electrodes after 2000 cycles.

8) Comparison of the reported supercapacitors

Table S1: Supercapacitor properties of the materials reported in the literature and obtained from this study

Material	Specific capacitance, [F g^{-1}]	Energy density [Wh kg^{-1}]	Power density [kW kg^{-1}]	Stability [%] (Cycles)	Ref.
		MoS_2 composite with graphene or modified graphene			
2D MoS_2@rGO	265	63		92 (1000)	[3]
MoS_2@chemically modified graphene	257	-	-	93 (1000)	[4]
MoS_2@GNS	282	-	-	93 (1000)	[5]
MoS_2@G	270	12.5	2.5	89.6 (1000)	[6]
MoS_2@N-G	245	-	-	91.3 (1000)	[7]
MoS_2@G*	46* (50[a])	7*[c]	3.5*[e]	240* (3500)	[8]
MoS_2@S-rGO*	6.56*[a]	0.58*[d]	13.4*[f]	91* (1000)	[9]
MoS_2@rGO*	30*[b]	-	-	-	[10]
MoS_2@rGO	**1064 (4,700[a])**	**47.6 (66.8[c])**	**7.63 (3.7[d])**	**95 (2000)**	**This work**

MoS_2 composite with carbon					
MoS_2@C	210	-	-	105 (1000)	[11]
MoS_2@C	589	72.7	12	104 (2000)	[12]
MoS_2@N-C	158	-	-	89 (1000)	[13]
MoS_2@C	201	-	-	94.1 (1000)	[14]
MoS_2@MPC	189	-	-	98 3000	[15]
MoS_2/graphene* membranes	4.29*[a]	-	-	~250* (10 000)	[16]
MoS_2 composite with polymer					
PPY@MoS_2	554	49.2	5.8	90 (500)	[17]
PANI@ MoS_2	552	-	-	79 (6000)	[18]
PANI@ MoS_2	853	-	-	91 (4000)	[19]
PANI@ MoS_2	567	-	-	92 (500)	[20]
PPy@ MoS_2	700	83.3	3.33	85 4000	[21]
MoS_2@PANI	390	-	-	86 (1000)	[22]
PANI@MoS_2@C	678	-	-	80 (10,000)	[23]
MoS_2 composite with metal oxide/sulfide					
CeO_2@MoS_2	102[a]	84[b]	3.5[e]	94 (2000)	[24]
Ni_3S_4@MoS_2	1441	-	-	90.7 (3000)	[25]
Ni_3S_2@MoS_2	1165	-	-	91 (2000)	[26]
MoS_2@$Ni(OH)_2$*	516*	5.2*[c]	11*[f]	94.2 (9000)	[27]

* Values from supercapacitor device,

a: [mF cm^{-2}], b: [F/cm^{3}]; c: [µWh cm^{-2}], d: [mWh cm^{-3}], e: [mW cm^{-2}], and f: [W cm^{-3}]

9) Supercapacitive properties of asymmetric supercapacitors (ASCs) MoS_2// rGO:

Electrochemical studies of the MoS_2//rGO ASC device: cyclic voltammograms at various potential ranges from 0.8 to 1.8 V in PVA-KOH gel electrolyte at a scan rate of 100 mV s−1, voltammetric response of MoS_2//rGO ASC device at different scan rates, galvanostatic charge-discharge curves of

MoS_2//rGO within the potential range 1.6 V at different current densities, and Ragone plot for MoS_2//rGO ASC device at different current densities. Inset fig d shows capacitance retention of ASC.

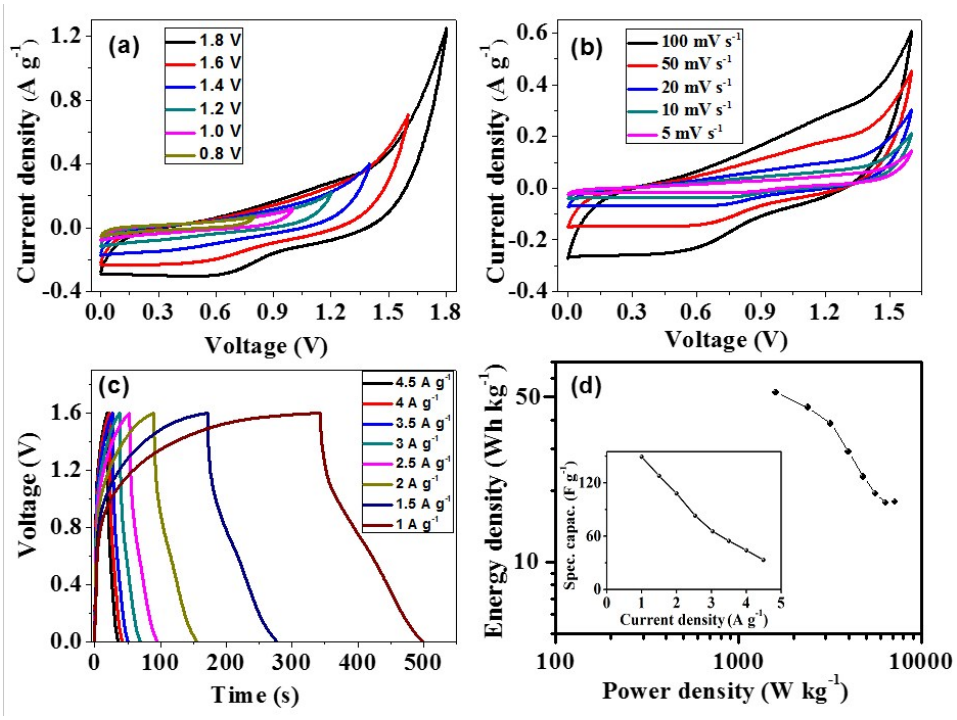

Fig. S7: Electrochemical studies of the MoS_2//rGO ASC device: (a) cyclic voltammograms within the various potential ranges from 0.8 to 1.8 V in PVA-KOH gel electrolyte at a scan rate of 100 mV s−1, (b) voltammetric response of MoS2//rGO ASC device at different scan rates, (c) galvanostatic charge-discharge curves of MoS_2//rGO within the potential range 1.6 V at different current densities, and (d) Ragone plot for MoS_2//rGO ASC device at different current densities. The inset of (d) shows the variation of the specific capacitance with different current densities.

10) EIS and Stability studies of MoS_2// rGO:

The Nyquist plot of MoS_2//rGO ASC device and stability studies for 2000 cycles at the current density 4.5 A g^{-1}.

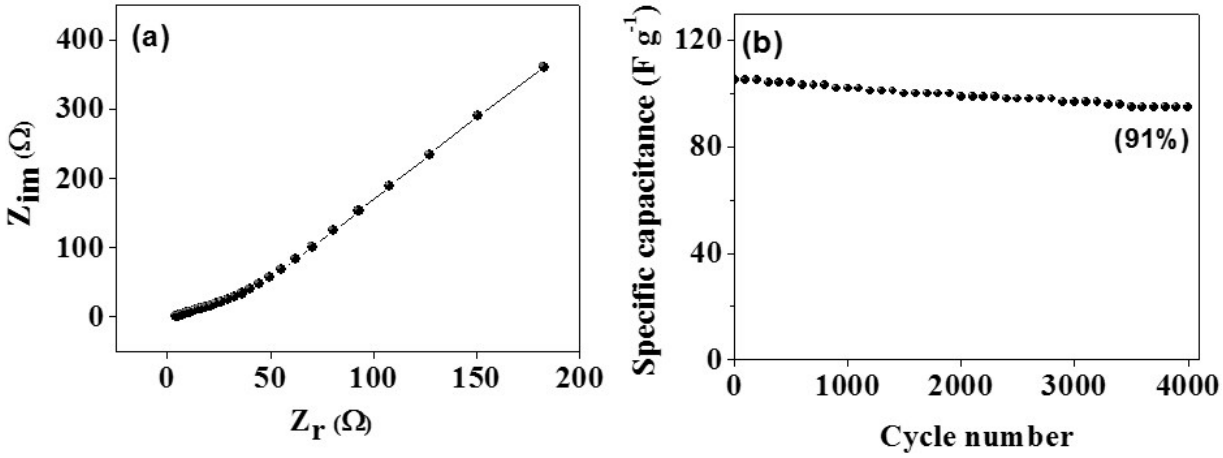

Fig. S8: Nyquist plot of MoS_2//rGO ASC device over the frequency range, 10 MHz to 0.01 Hz (a) and cyclic stability of MoS2//rGO ASC device for 4000th cycles (b).

Notes and References:

1 Y.F. Nicolau, Applications of Surface Science, 1985, 22/23, 1061-1074.

2 R. N. Bulakhe, S. Sahoo, T. T. Nguyen, C. D. Lokhande, C. H. Roh, Y. R. Lee and J.-J. Shim, *RSC Adv.*, 2016, **6**, 14844-14851.

3 E. G. Silveira Firmiano da, A. C. Rabelo, C. J. Dalmaschio, A. N. Pinheiro, E. C. Pereira, W. H. Schreiner and E. R. Leite, *Adv. Energy Mater.*, 2013, **4**, 1301380.

4 M. H. Yang, J. M. Jeong, Y. S. Huh and B. G. Choi, *Compos. Sci. Technol.*, 2015, **121**, 123-128.

5 S. Patil, A. Harle, S. Sathaye and K. Patil, *Cryst. Eng. Comm.*, 2014, **16**, 10845–10855.

6 R. Thangappan, S. Kalaiselvam, A. Elayaperumal, R. Jayavel, M. Arivanandhan, R. Karthikeyan and Y. Hayakawa, *Dalton Trans.*, 2016, **45**, 2637–2646.

7 B. Xie, Y. Chen, M. Yu, T. Sun, L. Lu, T. Xie, Y. Zhang and Y. Wu, *Carbon*, 2016, **99,** 35-42.

8 N. Savjani, E. A. Lewis, M. A. Bissett, J. R. Brent, A. W. Dryfe Robert, S. J. Haigh, and P. O. Brien, *Chem. Mater.*, 2016, **28,** 657−664.

9 X. Yuxiu, H. Lei, Z. Qi, X. Shuhua, C. Qi and S. Wangzhou, *Appl. Phys. Lett.,* 2015, **107**, 0139061-0139065.

10 S. Gengzhi, L. Juqing, Z. Xiao, W. Xuewan, L. Hai, Y. Yang, H. Wei, Z. Hua and C. Peng, *Angew. Chem*., 2014, **126,** 12784 –12788.

11 B. Hu, X Qin, A. M. Asiri., A. A. Khalid, A. O. Al-Youbib and X. Sun, *Electrochim. Acta*, 2013, **100**, 24– 28.

12 J. Hongmei, C. Liu, T. Wang, J. Chen, M. Zhengning, J. Zhao, W. Hou and G. Yang, *Small*, 2015, **11(48),** 6480–6490.

13 M. H. Yang, S. K. Hwang, J. M. Jeong, Y. S. Huh and B. G. Choi, *Synthetic Met.*, 2015, **209**, 528–533.

14 L. Q. Fan, G. J. Liu, C. Y. Zhang, J. H. Wu and Y. L. Wei, *Int. J. hydrogen Energ.,* 2015, **40**, 10150 -10157.

15 Q. Weng, X. Wang, X. Wang, C. Zhang, X. Jiang, Y. Bando and D. Golberg, *J. Mater. Chem. A*, 2015, **3,** 3097–3102.

16 M. A. Bissett, I. A. Kinloch and A. W. Dryfe Robert, *ACS Appl. Mater. Interfaces*, 2015, **7**, 17388−17398.

17 S. Faraji and A. F. Nasir, *Renew. Sust. Energ. Rev.* 2015, **42**, 823–834.

18 L. Ren, G. Zhang, Z. Yan, L. Kang, H. Xu, F. Shi, Z. Lei and Z. H. Liu, *ACS Appl. Mater. Interfaces*, 2015, **7**, 28294−28302.

19 J. Zhu, W. Sun, D. Yang, Y. Zhang, H. H. Hoon, H. Zhang and Q. Yan, *Small*, 2015, **11(33),** 4123–4129.

20 K. Gopalakrishnan, S. Sultan, A. Govindaraj and C.N.R. Rao, *Nano Energy*, 2015, **12**, 52–58.

21 H. Tang, J. Wang, H. Yin, H. Zhao, D. Wang and Z. Tang, *Adv. Mater*., 2015, **27**, 1117–1123.

22 J. Wanga, Z. Wu, K. Hu, X. Chen and H. Yin, *J. Alloys Compd.*, 2015, **619**, 38–43.

23 C. Yang, Z. Chen, I. Shakir, Y. Xu and H. Lu, *Nano Res.*, 2016, DOI.10-1007/s12274-016-0983-3.

24 N. Li, H. Zhao, Y. Zhang, Z. Liu, X. Gong and Y. Du, *Cryst. Eng. Comm.*, 2016, 10.1039/c5ce02466h.

25 Z. Yu, S. Wenping, R. Xianhong, L. Bing, T. T. Hui, G. Guilue, M. Srinivasan, Z. Yun and Y. Qingyu, *Small*, 2015, **11(30)**, 3694–3702.

26 J. Wang, D. Chao, J. Liu, L. Lic, L. Lai, J. Lina and Z. Shen, Nano Energy, 2014, 7, 151–160.

27 C. Hao, F. Wen, J. Xiang, L. Wang, H. Hou, Z. Su, W. Hu and Z. Liu, Adv. Funct. Mater., 2014, 24, 6700–6707.